Nuclear Science and Techniques (2024) 35:176
https://doi.org/10.1007/s41365-024-01524-z

Research and development of a 0.5-m-long helical superconducting undulator prototype

Xiang-Chen Yang[1,2] · Xiao-Wu Yu[3] · Jun-Hao Wei[4] · Xiang-Zhen Zhang[2] · Zi-Lin Chen[2,4] · Xiao-Juan Bian[2] · He-Ting Li[1] · Guang-Yao Feng[1] · Yu-Hui Li[2]

Received: 6 December 2023 / Revised: 28 February 2024 / Accepted: 10 March 2024 / Published online: 25 September 2024

Abstract
The helical undulator is in high demand in synchrotron radiation facilities for circular polarization generation. Owing to the higher field strength provided by the superconducting undulator compared to the conventional permanent-magnet undulator, greater research efforts should be directed toward this area. The helical superconducting undulator holds great potential in synchrotron radiation facilities, especially in low-energy storage rings that seek circularly polarized radiation with the highest possible radiation flux. Following the successful development of planar superconducting undulators, the Institute of High Energy Physics conducted research and development for the helical superconducting undulator. A 0.5-m-long Delta-type superconducting undulator prototype was developed and tested. Detailed information on the design, fabrication, and cryogenic testing of the prototype is presented and discussed.

Keywords Helical · Superconducting undulator · Delta

1 Introduction

Four generations of light sources have been developed since the observation of synchrotron radiation (SR). The fourth-generation light sources significantly reduce the electron beam emittance by utilizing multi-bend achromatic technology [1]. This advancement enables diffraction-limited SR and supports multi-disciplinary research in fields such as atomic and molecular optics, condensed-matter physics, materials science, chemistry, and life sciences. Because of its unprecedented features and advantages, fourth-generation light sources have attracted increased attention worldwide, leading to the construction of numerous facilities such as MAX-IV in Sweden, Sirius in Brazil, ESRF-EBS in France, APS-U in the USA, HEPS in Beijing, and HALF in Hefei, China. For all advanced light sources, an essential insertion device, known as an undulator, is used to generate radiation [2]. The quality of the undulator largely determines the functionality of the radiation facility.

An undulator is a magnetic device consisting of periodic magnetic arrays that generate a field that alternates periodically along the beam transport direction. There are two types of undulators, planar and helical. A planar undulator produces a single-direction field, typically in the vertical direction. Electrons oscillate horizontally through a planar undulator, resulting in a linearly polarized radiation. In contrast, the helical undulator (HU) was developed to generate a periodic magnetic field in both the vertical and horizontal directions. It exhibits a tunable phase shift, allowing switchable polarization. The HU has diverse research applications including the study of chiral molecules utilizing radiation with variable polarization [3]. Circularly polarized radiation is valuable for investigating information storage in magnetic materials. By adjusting the polarization, changes

This work was supported by the National Natural Science Foundation of China (No. E1113R5C10).

✉ Yu-Hui Li
liyuhui@ihep.ac.cn

[1] National Synchrotron Radiation Laboratory, University of Science and Technology of China, Hefei 230029, China

[2] Institute of High Energy Physics, Chinese Academy of Sciences, Beijing 100049, China

[3] Institute of Plasma Physics, Chinese Academy of Sciences (ASIPP), Hefei 230031, China

[4] China Spallation Neutron Source, Institute of High Energy Physics, Chinese Academy of Sciences, Dongguan 523000, China

in the magnetization can be observed, leading to innovative methods and materials for faster and more condensed storage devices. In addition, the HU can generate vortex light with orbital angular momentum (OAM) [4], which is particularly useful for research on X-ray absorption spectra. Both APPLE and Delta undulators can function as an HU. The APPLE undulator provides an open aperture horizontally, but has a limited aperture vertically. In contrast, the Delta undulator restricts its aperture in both the vertical and horizontal directions [5]. Owing to the advantages of fourth-generation light sources, the beam size in both the vertical and horizontal planes is small, making the Delta undulator a suitable option.

Currently, the most commonly used insertion device is the permanent-magnet undulator (PMU), which utilizes high-remnant-magnetization materials such as NdFeB and PrFeB. PMU technology is becoming increasingly mature, and the maximum field it can achieve is reaching its limit. Moreover, it is important to note that permanent-magnet materials are sensitive to radiation hazards and may be demagnetized. With the rapid development of superconducting magnet technology for accelerators, superconducting undulators (SCUs) have gradually gained popularity. Currently, with the available technology, SCUs are capable of providing a comparable field even in the short-period range of 10–15 mm. As the period increases, the magnetic field produced by the NbTi material used in the SCU becomes significantly larger than that produced by the cryogenic PMU (CPMU) [6]. Therefore, SCUs maintain priority in terms of field strength. Additionally, they have the advantage of being able to withstand radiation damage, surpassing PMUs. Substantial progress has been achieved in SCU development in recent years, particularly through research conducted at institutions such as the KIT in Germany and the Argonne National Laboratory in the USA [7, 8]. The APS-U project at Argonne is expected to utilize a large number of SCUs. However, research on SCU in China is still in its early stages, with limited experimental trials conducted at the Shanghai Synchrotron Radiation Facility (SSRF) and the Institute of High Energy Physics (IHEP). In 2021, the SSRF successfully developed a 0.8-m-long prototype that operates with beams [9]. In 2022, the IHEP successfully developed a 1.5-m-long planar SCU with a 9.5-mm gap and a maximum excitation current of 450 A. The magnetic field was measured at currents of 400 A and below, revealing a maximum phase error of 8.3° [10].

A new SR facility, HALF, has been approved and is currently under construction in Hefei, China. In Phase I, ten beamlines and 13 insertion devices will be built [11]. More than half of the undulators are circularly polarized. This includes one with a six-array structure designed as a Spring-8 type undulator [12], which is used for energy conversion and celestial chemical ionization mass spectrometry with the specific goal of emitting radiation in a pure circular polarization state. In addition, there are six EPUs with switchable polarization for research on electronic states, spatiotemporal resolution, and microscopic imaging. All these undulators are of the PMU type, and polarization tuning is achieved by mechanically shifting the magnet girders. Additionally, the field strength must be adjusted by changing the gaps. Mechanical movement complicates undulator design and increases costs [13]. Despite these efforts, the degree of polarization varies only by changing the gap, thus degrading the field quality. In comparison, SCUs stand out from PMUs owing to its convenient polarization switch by varying the excitation current without any mechanical movement. All polarization states are available, including the horizontal linear polarization (HLP), vertical linear polarization (VLP), left circular polarization (LCP), and right circular polarization (RCP) [14]. Therefore, a helical SCU is urgently required in Phase II of HALF to advance circular polarization generation. This prospect has motivated the study of helical SCU, as described in this paper.

Two coil winding techniques are available for generating circular polarization in an SCU: the double-helix coil [15, 16] and the Delta structure. The double-helix coil has a simpler structure with two sets of co-wound coils, in which the current flows in opposite directions. However, it provides only circular polarization and lacks the ability to generate linear or elliptical polarization. By contrast, the Delta-type helical SCU resembles the structure of a Delta PMU consisting of four parallel parts [17]. These four parts are grouped into two pairs, with each pair comprising two opposing parts. As shown in Fig. 1, the pair of left-right parts generates a horizontal field, whereas the other pair of up-down parts generates a vertical field. The displacement between these two pairs is fixed, indicating that it is not possible to generate an elliptical polarization with a tilted axis.

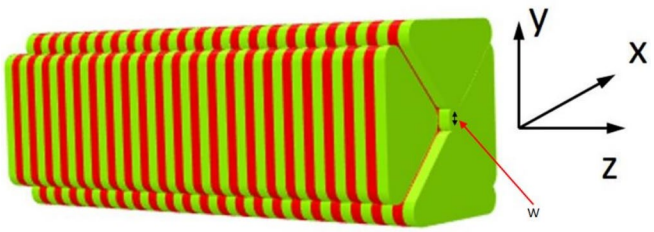

Fig. 1 (Color online) Simulation model of the Delta-type SCU

B_y is used to address the vertical field and B_x is used for the horizontal field:

$$B_y = B_{y0}\cos\frac{2\pi z}{\lambda_u}, \tag{1}$$

$$B_x = B_{x0}\cos\left(\frac{2\pi z}{\lambda_u} + \frac{\pi}{2}\right), \tag{2}$$

B_{y0} and B_{x0} are the peak fields, z indicates the longitudinal (undulator axis) direction, and λ_u is the period length. The phase between B_x and B_y is fixed at $\pi/2$, which is the result of a structural shift in a quarterly period. Each pair of magnetic parts is independently excited by a power supply, allowing for flexible combinations of B_x and B_y in terms of field strength and direction. The Stokes parameters can be adjusted accordingly, enabling the achievement of a variety of polarized states, including HLP, VLP, LCP, and RCP.

This paper focuses on a Delta-type helical SCU prototype developed at IHEP.

2 Physical design of the Delta-type SCU

The Delta-type SCU simulation model is shown in Fig. 1. The iron core composed of DT4 is highlighted in green. The superconductor coil, composed of NdTi, is shown in red. The iron core was designed with grooves to accommodate the coil winding, and the protrusions of these grooves act as poles that conduct the magnetic flux and enhance the field strength. The width and depth of the grooves were meticulously adjusted to optimize the magnetic field. Each magnetic part has a trapezoidal cross section, and the gap in the middle serves as the pathway for the beams. The width of the top distance in the trapezoid determines the size of the undulator gap [18], represented as W. W is a critical parameter for the Delta-type SCU; in our optimization, W is set to 6 mm to achieve a small gap with sufficient field.

Many users are satisfied with the linear polarization of hard X-rays; however, users working with soft X-rays often require the ability to control polarization, including circular polarization. The resonance condition of undulator radiation indicates that the lower photon energies of soft X-rays require longer undulator periods. Considering the potential requirements in Phase II of HALF, a 28-mm period was chosen for the Delta-type SCU prototype.

Two shapes of superconductive wires are available in the market: round and rectangular. The SCU requires flexibility of the winding in all directions, allowing for an alternative current direction from groove to groove. Therefore, a round shape is more suitable. The Cu:Sc ratio is another important parameter. Cu is soft, whereas NbTi is stiff. A higher fraction of Cu enhances the flexibility but decreases the maximum current. SSRF chose Cu:Sc ratios of 0.93 and 1.3 [19–21], while IHEP used ratios of 0.9 and 0.6 in its previous studies. With the developed knowledge, the IHEP is able to wind an SCU with a low Cu:Sc ratio, pursuing a high current with a stiff wire. A diameter of 0.6 mm was chosen as the thickness at which each groove could accommodate a sufficient number of wires [22].

To develop the Delta-SCU winding technology on a limited budget, a 0.5-m-long prototype was manufactured. The gap between the opposite poles was set at 12 mm, and the coil groove cross section was measured as 7 mm × 6 mm in width and depth, respectively. The coil was wound in each groove, starting from the bottom and progressing to the top. The winding number varied between the layers [23], with 11 and 10 alternating turns. There were nine layers in total, with five layers having 11 turns and four layers having 10 turns. Each groove has 95 wound turns. The magnetic field produced by this configuration was calculated using the OPERA-3D code.

The ending-field design in an SCU requires special consideration. Depending on the field polarity on both sides, the ending field can be categorized as symmetric or anti-symmetric. At the symmetric ending, the polarized fields are the same on both sides, and the center of the undulator corresponds to the peak of the magnetic field. In contrast, the anti-symmetric undulator has opposite polarization on both sides, and the field crosses zero at the undulator center [24]. In our design, we selected the anti-symmetric configuration, where the residual field integrals in the entrance and exit ends cancel each other out in the ideal case, which is the most commonly adopted approach in undulator design. Based on the selected ending-field design and considering a total length of 0.5 m and a period of 28 mm, each magnetic part consists of 31 coil grooves.

Although simulations show a satisfactory field performance with small errors that meet scientific requirements, field imperfections are inevitable during practical fabrication. These imperfections lead to first and second field integral errors. To rectify these errors, independent coils were wound at both ends of the main SCU coil [25]. These coils are excited by separate power supplies, and the field error can be reduced based on measurements. Corrector ending coils have been proven to be effective in reducing field errors, as demonstrated in the planar SCU prototype [26].

Superconductivity is determined by three crucial parameters: the loading current, magnetic field, and temperature. In most cases, the SCU is cooled to a fixed liquid helium temperature of 4.2 K. The maximum loading current is dependent on the magnetic field; higher currents generate higher fields in the coils, which in turn decreases the current that can be loaded. The load line for the Delta-SCU is shown in Fig. 2, where the blue line represents the critical current relative to the magnetic field based on the

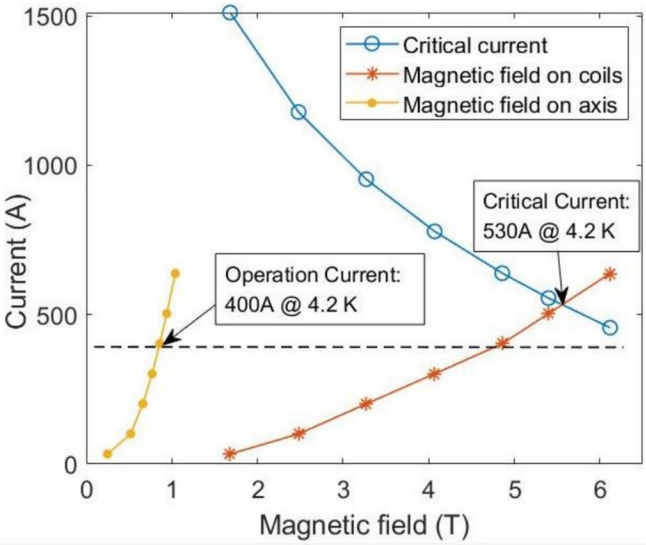

Fig. 2 (Color online) Load line of the Delta-type SCU

Table 1 Delta-type SCU parameters

Parameter	Value
Cu:Sc ratio	0.9
Iron core material	DT4
Period length (mm)	28
Period number	16
Magnetic gap (mm)	12
Operating current (A)	400
Central peak field (T)	0.85

adopted NbTi wire. The red line represents the calculated SCU coil field for different loading currents. The intersection of the blue and red lines indicates the maximum loading current allowed in the SCU, 530 A. Additionally, the yellow line represents the undulator field at the gap center for different loading currents. According to the load line, the SCU can achieve a maximum peak magnetic field of 0.98 T@530 A along the axis. To achieve the designed magnetic field, the operating current was set to 400 A, which is approximately 75% of the critical value.

The Delta-type SCU prototype parameters are listed in Table 1

As described previously, a Delta-SCU is composed of four parts divided into two pairs: up-down and left-right. Each pair is powered independently. The polarization can be adjusted by applying different currents to each pair. For instance, circular polarization requires equal currents in both pairs; vertical linear polarization requires full current in the left-right pair and zero current in the up-down pair; and horizontal linear polarization requires full current in the up-down pair and zero current in the left-right pair. Additionally, different current combinations applied to the coil pairs can produce various elliptical polarization states.

3 Mechanical structure and technology

The iron core serves as the backbone for each part of the magnet, around which the NbTi superconducting wire is wound. These four parts are mechanically fixed to a common structure. The formal SCU is expected to be assembled into a cryostat based on zero-liquid helium consumption technology. Considering the impact of the beam heat load on magnet stability, a separate vacuum chamber needs to be designed [27–29]. To maximize the achievable field strength, the gap is designed to be as small as possible, which prevents the use of conventional cooling technology for the liquid helium bath because it occupies extra space in the form of the helium tank [30, 31]. Instead, a cooling technique utilizing the "thermosiphon" effect is employed. In this technique, liquid helium is circulated using a thermal gradient, thereby eliminating the need for a pump. A channel is machined at the center of the iron core of each magnetic part to allow for the passage of liquid helium, enabling conduction cooling of the coil to the appropriate temperature for superconductivity [32].

Undulators require a qualified field that provides both high field strength and precision. This implies that fields must be identical from one period to another. During the transition from ambient to superconducting state, and considering the constraints that movable poles cannot be used for field error correction in the SCU and the irreversible nature of the process, strict control over the precision of fabrication steps, including machining of the iron core and poles, component assembly, and superconducting wire winding in the SCU, is essential. This is the main reason why it is more difficult to develop SCUs than PMUs.

The sinusoidal field of the SCU is generated by reversing the current direction in the adjacent grooves. This requires the NbTi wire to be wound in the direction opposite to that

of the groove. There are two available winding measures. In the first, the wire is initially wound in the odd-numbered grooves until the coil ends. Subsequently, the direction is reversed and is wound back from the end to the beginning in the even-numbered grooves. In the second measure, the wire is wound from groove to groove and the direction is reversed between each groove. The second measure is commonly used because of its superior feasibility. However, wire reversal between each groove poses a challenge. A method using a turn-around pin was suggested at Argonne Laboratory [33]; however, the turn-around pin size must be reduced for shorter periods, which leads to a new challenge: too small a bending radius while reversing directions would reduce the current-carrying capacity of the wire. To overcome this challenge, innovative technology using a wheel for wire reversal has been developed. The conductor wire passes through the wheel mounted on the G10 groove baffle plates [34]; thus, its radius can be kept the same for different period lengths, ensuring a sufficient bending radius and avoiding a decrease in the current-carrying capability. This structure is illustrated in Fig. 3.

Another technological challenge associated with SCUs is the insulation treatment between the conductor and iron core. The limited operational space within the grooves makes it difficult to adopt conventional insulation measures, such as wrapping fiberglass or Kapton, as these would greatly affect the winding accuracy and are heavily dependent on the operator. Although winding the wire directly on the polished iron core can ensure accuracy [35], this approach is mechanically challenging to implement, and any unpolished mechanical burrs may damage the wire insulation. Moreover, the outer insulating layer of the wire is less than 0.03 mm, coupled with the fallibility of the coating technology used, which means that the manufacturer cannot guarantee a uniform conductor insulation quality to meet the standard everywhere. These factors may lead to contact between the wire and iron core, significantly reducing the insulation grade or even resulting in a short circuit.

To minimize the insulation risks while achieving high mechanical precision, the iron core and poles were machined separately. The slots were cut on the iron to mount the poles, and each pole was positioned accurately using two pins. In the fabrication process, the iron core was first machined without pole slots and then coated with a 0.1-mm-thick G10 plate bonded with epoxy. A special mold was used to ensure a secure attachment between the G10 plate and the iron core. Subsequently, pole slots were machined onto the core. To ensure adequate insulation on the sides of each groove, two pieces of 0.2-mm-thick G10 plates were bonded to both sides of the poles and then assembled onto the iron core. Additional grinding ensured the mechanical accuracy and transition matching of the poles. The homogeneity of the magnetic field from one pole to another is crucial and depends on the overall flatness. After the poles were mounted, they were machined using a grinder. Through these procedures, the wire grooves were well-insulated with excellent mechanical precision. The coil groove width and pole flatness were measured in three coordinates, with a maximum error of approximately 50 microns in the groove width and a constraint of below 20 microns for the pole height error.

The field quality may be degraded owing to the iron core deformation under multiple magnetic forces. However, given the thinness of the iron core, the mechanical strength of the magnetic parts was much weaker than that of the PMU, despite both experiencing similar magnetic forces. This is a particularly challenging issue for the SCU. To address this issue, a robust stainless-steel board was designed to assemble the magnet. Each part was connected to its respective board through transition plates designed at both ends. After mounting the parts on the boards, four boards were assembled to form a robust surrounding structure capable of withstanding magnetic forces ranging from zero to several tons in different directions, as shown in the plots on the left side of Fig. 4. In addition, assembly errors can contribute to field errors. Positioning pins were designed and machined for each component to ensure sufficient accuracy. Additional positioning blocks were inserted between the magnetic part and board, as well as between two adjacent magnetic parts, to prevent mechanical deformation and maintain a consistent gap throughout the entire undulator.

Superconducting magnets must undergo excitation training prior to operation. During this process, the current gradually increases, leading to an increase in the magnetic field. Under these conditions, even slight movements between the wires owing to varying magnetic forces can cause quenching. The wire is tightened to minimize the likelihood of quenching. Owing to the unique structure of the SCU, it is not feasible to wrap an aluminum alloy pre-tightening layer around the coil or to design a pre-tightening structure similar to a superconducting wiggler to apply stress to the coil [36, 37]. The only available method is to impregnate epoxy into the coil, which solidifies the wire, enabling it to resist

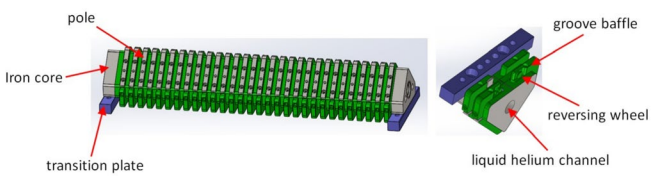

Fig. 3 (Color online) Structural design of the magnetic part

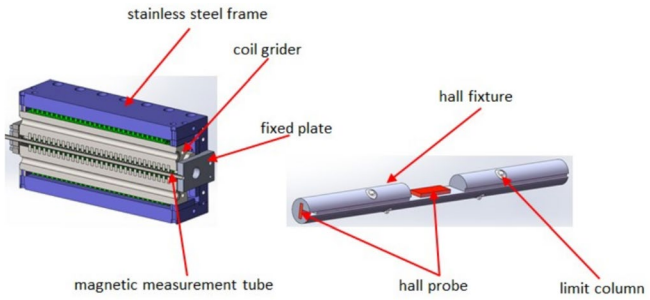

Fig. 4 (Color online) Structural design of the assembly and magnetic measurement

electromagnetic forces within a certain range and enhance the insulation effect. Therefore, epoxy vacuum impregnation was performed after coil winding. Owing to the varying shrinkage rates of the iron core, superconducting coil, and epoxy, cracks commonly appear in the epoxy after cooling. This issue not only impacts the appearance of the coils but also has several adverse effects owing to epoxy cracks. For instance, moisture from the air can seep into the coil through epoxy cracks, reducing the insulation grade between the coils and iron core. Furthermore, cracks can result in the release of heat and increase the likelihood of wire movement and quenching during excitation training. Consequently, the training process becomes more complex, leading to a proportional increase in cost and workload. For the SCU, it is important to emphasize that when the superconducting magnet is reheated to room temperature to adjust the mechanical parameters, the internal stress is redistributed throughout the entire coil due to the lack of a preload structure. This can cause secondary epoxy cracking, resulting in almost no memory effect from the previous training. Therefore, the influence of epoxy cracking on the SCU is more significant than that of the others.

Therefore, epoxy cracking must be carefully studied. After fabricating the four SCU parts, they were impregnated with epoxy resin. For comparison, no special treatment was applied to parts 1# and 2#, which were impregnated with an ordinary epoxy. Part 2# underwent a cooling test using two PT100 temperature sensors attached to the top and bottom surfaces. For convenience, liquid nitrogen was used in the test as the cooling medium. The magnetic part was placed above the liquid nitrogen, and its height was adjusted for temperature control. The rewarming and cooling rates can also be controlled by adjusting the speed at which the magnet rises and falls. The typical cooling speed for superconducting magnets is approximately 25 °C/h, which is the same value used for this test. The temperature variations are shown in Fig. 5, where the black and red curves represent the upper- and lower-side temperatures, respectively. It can be seen that the temperature of the two sensors initially decrease slowly at the expected rate. The sudden drop to approximately 77 K at approximately 4 h was due to the direct contact of the lower side with liquid nitrogen, which occurred almost instantaneously, while the upper surface remained exposed to the atmosphere. At approximately 6 h, the coil was immersed in liquid nitrogen. Subsequently, the coil was slowly removed from the liquid nitrogen, and the upper surface of the coil was first exposed to the atmosphere. However, the temperature of the entire coil must be

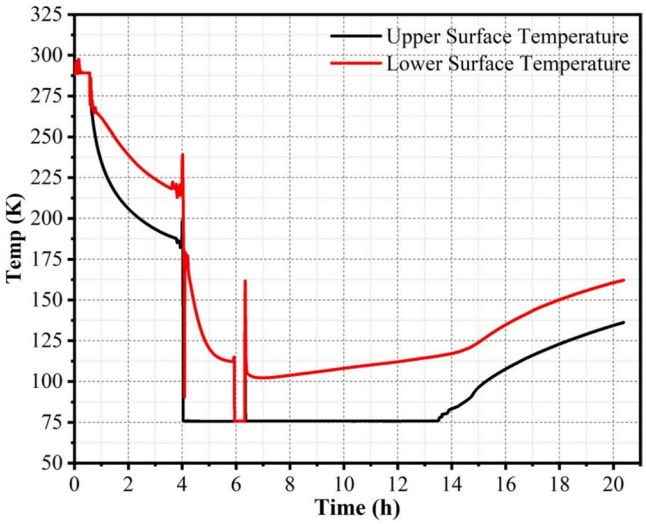

Fig. 5 (Color online) Temperature curve of the liquid nitrogen impact

balanced; therefore, the temperature slowly decreased after reaching a peak. After finishing the cooling test, two main features were observed: (i) many cracks appeared and (ii) there were more cracks on the upper side than on the lower side, despite the lower side experiencing a much quicker temperature drop owing to direct contact with liquid nitrogen. The difference between the upper and lower sides is the groove depth, as the upper side is deeper to accommodate the wire reversal wheel. Considering the NbTi wire as the filling material for the epoxy, the lower side had a higher filling factor than the upper side. Therefore, it is evident that the primary method for minimizing cracks is to incorporate the filling material into the epoxy. This conclusion is logical because the tensile strength of epoxy alone is relatively low but can be significantly bolstered by the addition of filling materials, akin to the reinforcing effect observed in reinforced concrete [38].

Subsequent attempts focused on applying filling materials to epoxy and observing their effects. In part 3#, a glass-fiber mat was used to fill the epoxy. The mat was cut into small pieces and placed in the grooves. In addition, a glass-fiber layer was applied outside part 3# to further increase the strength of the outermost epoxy. After coil impregnation and before the cooling-down process began, a significant reduction in the number of cracks was observed compared to the first two magnetic parts. However, some cracks remained on the upper side. In part 4#, glass powder was used as the filling material, which improved the filling homogeneity and filling factor. The powder particles have a diameter of 0.15 mm, which is much finer than that of the cut glass-fiber mat. It is worth noting that smaller particles should not be selected as they can be inhaled and are harmful. Following the epoxy impregnation of part 4#, no cracks were found, effectively addressing this issue.

4 Coil cryogenic test

A helium-free cryogenic platform was developed at the IHEP to test superconducting magnets [39]. It is powered by two 1.8-W cryocoolers with two-stage temperatures. The first stage of the cryocooler is connected to the inner cold shield and cooled below 60 K. The second stage provides a temperature below 4 K for superconductivity. A pair of binary current leads is installed on the flange, which could conduct currents up to 600 A. Each current lead is divided into two sections at high and low temperatures. The high-temperature section is connected to the first cryocooler stage, while the low-temperature section is connected to the second stage. The platform is equipped with a set of superconducting power supplies capable of providing a maximum excitation current of 580 A, along with a multi-channel quench protection system. As the platform does not require liquid helium for cooling, it offers convenience and cost savings. However, additional attention must be paid to ensure proper contact between different components for effective cooling. An unwanted contact must be avoided to ensure that the magnet is cooled to the desired temperature [40]. Considering the conduction heat leakage caused by the sensor wires, the local temperature at the lead-out position may be too high to transition to a superconducting state. Therefore, the thermal conductivity of the sensor wires should be carefully considered and addressed. During the installation process, all signal wires were arranged to dissipate heat at the first-/second-stage position of the cryocooler. The 0.5-m-long prototype can be cooled, excited, and trained on this platform.

Following the above-mentioned procedure, the four magnetic parts were wound and impregnated. Two parts were impregnated without any filling, another part was impregnated with small pieces of glass-fiber mat, and the remaining part was impregnated with glass-fiber powder. To investigate the effects of cracks and epoxy filling on quenching during excitation training, parts 1# and 4# without filling and with fiber powder filling, respectively, were selected for comparison. The excitation training for the two parts was conducted separately.

The quench number and current were recorded, as shown in Fig. 6. The blue curve represents part 4# with fiber powder filling, whereas the red curve represents part 1# without filling. It is evident that part 4# significantly outperforms part 1#, as evidenced by its much lower quench number and the ability to handle a higher maximum current. For

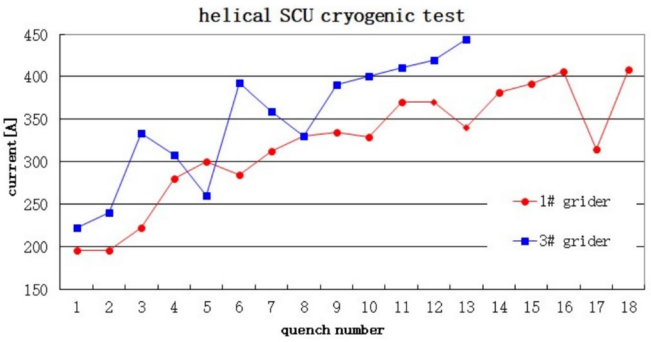

Fig. 6 (Color online) Training curves for the superconducting coils

the design goal of 400 A, part 4# experienced six quenches, while part 1# experienced 15 quenches. The maximum loading current for part 4# was approximately 450 A, compared to slightly over 400 A for part 1#.

A visual comparison between the two magnetic parts after completing the cryogenic test is shown in Fig. 7. Because of the excessive epoxy shrinkage after the temperature was reduced to 4.2 K, part 4# was visibly cracked after cryogenic excitation, even though there were no cracks after epoxy impregnation. However, compared with part 1#, the epoxy cracks in part 4# were significantly reduced and mainly concentrated on the surface, and the depth and width were also significantly improved. Although the problem of cryogenic cracking in coil epoxies has not been completely resolved, significant success has been achieved in reducing the extent of this phenomenon. These test results confirm the importance of minimizing epoxy cracks and the significance of the filling measures developed through prototype research.

However, the test platform could only accommodate the excitation training of the coils and magnetic field measurements could not be conducted. To obtain the magnetic field quality of the prototype, it is necessary to perform Hall point measurements using a vertical measurement dewar using the liquid helium bath method. A similar system was developed for planar SCU measurements [41]. Considering the potential of magnetic field measurements, we designed a corresponding magnetic measurement structure.

Figure 4 illustrates this design. A high-precision magnetic measurement tube is installed in the magnetic gap. To ensure high positional accuracy, the two ends of the tube are connected to a fixed plate, which is in turn connected to a stainless-steel board secured by pins. Two hall probes are mounted perpendicularly in the middle of the cylindrical fixture to measure the horizontal and vertical fields, and slots are cut on the outer surface to accommodate signal wires [42, 43]. Additionally, radial limits are placed on the surface of the cylindrical fixture, allowing flexible positioning using copper springs. Owing to the small radial dimension, the limits are arranged asymmetrically in the axial direction, enabling the fixture to slide through the undulator for field measurements with high position accuracy. As this study mainly focused on the optimization of the physical design and technological research on the helical SCU, addressing technological challenges such as precision winding, assembly, and epoxy cracking, the magnetic field measurement was not the primary focus. Furthermore, the measurement cost of the liquid helium bath method must also be considered. Therefore, related work on magnetic field measurements was not conducted.

5 Summary

SCUs have the potential to generate stronger fields than PMUs and offer better resistance against radiation damage. Delta-type helical SCUs allow various polarizations by adjusting the loaded current in different magnetic parts, enabling pure circular polarization, vertical/horizontal linear polarization, and multiple elliptical polarizations. The potential application of helical SCUs in Phase II of HALF in Hefei, China, is currently under consideration. A 0.5-m-long prototype of the Delta-type SCU was developed at IHEP, with four magnetic parts wound and impregnated. Extensive research was conducted to ensure the accuracy of the winding and assembly, and special measures were taken to increase the insulation grade. Furthermore, to examine the impact of epoxy cracking, a series of experiments were conducted, and the excitation training results for the two magnetic parts impregnated with and without filling material were compared, offering valuable insights into the effect of epoxy cracking. A wealth of knowledge has been gained via

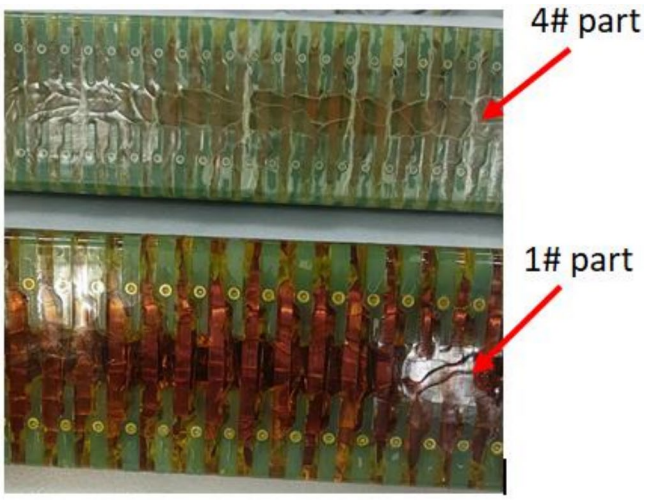

Fig. 7 (Color online) Epoxy cracking comparison after the cryogenic test

this development process, which is crucial in guaranteeing the future production of full-sized helical SCUs.

Author contributions All authors contributed to the study conception and design. Material preparation, data collection and analysis were performed by Xiang-Chen Yang, Xiao-Wu Yu and Jun-Hao Wei. The first draft of the manuscript was written by Xiang-Chen Yang. Coil testing was done by Xiang-Zhen Zhang, Zi-Lin Chen and Xiaojuan Bian. Idea and experimental program was proposed by Guang-Yao Feng, He-Ting Li and Yu-Hui Li. Manuscript revision was done by Yu-Hui Li. All authors commented on previous versions of the manuscript. All authors read and approved the final manuscript.

Data availability The data that support the findings of this study are openly available in Science Data Bank at https://cstr.cn/31253.11.sciencedb.j00186.00158 and https://www.doi.org/10.57760/sciencedb.j00186.00158.

Declarations

Conflict of interest The authors declare that they have no Conflict of interest.

References

1. P.H. Yang, Z.H. Bai, T. Zhang et al., Design of a hybrid ten-bend-achromat lattice for a diffraction-limited storage ring light source. Nucl. Instrum. Meth. A **943**, 162506 (2019). https://doi.org/10.1016/j.nima.2019.162506
2. N.A. Vinokurov, E.B. Levichev, Undulators and wigglers for the production of radiation and other applications. Physics Uspekhi **58**, 850–871 (2015). https://doi.org/10.3367/UFNe.0185.201509b.0917
3. R. Streubel, C.H. Lambert, N. Kent et al., Experimental evidence of chiral Ferrimagnetism in amorphous GdCo films. Adv. Mater. **30**, e1800199 (2018). https://doi.org/10.1002/adma.201800199
4. M. Padgett, J. Courtial, L. Allen et al., Light's orbital angular momentum. Phys. Today **57**, 35–40 (2004). https://doi.org/10.1063/1.1768672
5. H.D. Nuhn, S.D. Anderson, R.N. Coffee et al., Commissioning of the delta polarizing undulator at LCLS. Proceedings of the 37th international free electron laser conference, Daejeon, Korea, 757–763 (2015). https://accelconf.web.cern.ch/FEL2015/papers/wed01.pdf
6. J. Bahrdt, E. Gluskin, Cryogenic permanent magnet and superconducting undulators. Nucl. Instrum. Methods **907**, 149–168 (2018). https://doi.org/10.1016/j.nima.2018.03.069
7. S. Casalbuoni, A. Cecilia, S. Gerstl et al., Overview of the superconducting undulator development program at ANKA. AIP Conf. Proc. **1741**, 020002 (2016). https://doi.org/10.1063/1.4952781
8. M. Kasa, E. Anliker, Q. Hasse et al., Design, fabrication, and testing of a 1.9-m-Long, 1.65-mm period NbTi superconducting undulator for the advanced photon source upgrade. IEEE T. Appl. Supercon. **32**, 4101805 (2022). https://doi.org/10.1109/TASC.2022.3164039
9. J. Xu, Q. Zhou, L. Yin et al., Development of a superconducting undulator prototype at the SSRF. IEEE T. Appl. Supercon. **27**, 4100304 (2017). https://doi.org/10.1109/TASC.2016.2632758
10. J.H. Wei, X.C. Yang, Z.L. Chen et al., Development of NbTi planar superconducting undulators at the IHEP. Front. Phys. **11**, 1153005 (2023). https://doi.org/10.3389/fphy.2023.1153005
11. Z.Y. Zhao, Y.F. Xu, H.T. Li, Preliminary design of insertion devices at Hefei Advanced Light Facility. 14h Particle Accelerator Conference, Venice, Italy, 1247-1249 (2023). https://doi.org/10.18429/JACoW-IPAC2023-MOPM115
12. T. Hara, T. Tanaka, T. Tanabe et al., SPring-8 twin helical undulator. J. Synchrotron Rad. **5**, 426–427 (1998). https://doi.org/10.1107/s0909049597015719
13. Q.G. Zhou, M. Zhang, Y. Li et al., An APPLE-II type helical undulator for SSRF. APAC 2007. 714-716 (2007). https://doi.org/10.18429/JACoW-APAC2007-THPMA062
14. N. Yang, Y. Xu, Z. Zhao et al., Polarization switching of segmentally helical undulators in a diffraction-limited storage ring. Phys. Rev. Accel. Beams **26**, 080701 (2023). https://doi.org/10.1103/PhysRevAccelBeams.26.080701
15. S.H. Kim, Parameterization of helical superconducting undulator magnetic field. Proceedings of the North American Particle Accelerator Conference, Chicago, IL, USA, October 9–14, 2016. pp. 894–896. https://doi.org/10.18429/JACoW-NAPAC2016-WEPOB06
16. A. Hinton, B. Shepherd, Design of a short-period helical undulator. 12th Int. Particle Acc. Conf. 3844–3847 (2021). https://doi.org/10.18429/JACoW-IPAC2021-THPAB045
17. A. Temnykh, M. Babzien, D. Davis et al., Delta undulator model: magnetic field and beam test results. Nucl. Instrum. Methods **649**, 42–45 (2011). https://doi.org/10.1016/j.nima.2010.11.011
18. H.D. Nuhn, S. Anderson, G. Bowden et al., R &D towards a Delta-type undulator for the LCLS. 35rd International Free Electron Laser Conference, New York, NY, August 25-29, 2013. SLAC-PUB-15743, (2013). https://www.slac.stanford.edu/pubs/slacpubs/15500/slac-pub-15743.pdf
19. Y.Y. Liu, L. Wang, J. Wang et al., Study on cooling technology of the superconducting undulator at SSRF. Proc. 10th mechanical engineering design of synchrotron radiation equipment and instrumentation (MEDSI'18), Paris, France, 25-29 June 2018. 75-77 (2018). https://doi.org/10.18429/JACoW-MEDSI2018-TUPH22
20. Z. Zhang, Y. Jiang, W. Zhang et al., Design and test of a superconducting undulator mock-up coil at SSRF. IEEE T. Appl. Supercond. **24**, 4101503 (2014). https://doi.org/10.1109/TASC.2013.2293890
21. L. Wang, Y. Liu, X. Guo et al., Development of a test cryostat for a superconducting undulator prototype at the SSRF. IEEE T. Appl. Supercond. **31**, 9500105 (2021). https://doi.org/10.1109/TASC.2021.3055168
22. J.H. Wei, C.D. Deng, L.L. Gong et al., Design of a Delta-type superconducting undulator at the IHEP. Proceedings of the 12th international particle accelerator conference. 2391–2393 (2021). https://doi.org/10.18429/JACoW-IPAC2021-TUPAB373
23. S. M. Lynam , R. Agustsson, I.I. Gadjev et al., Fabrication progress of a superconducting helical undulator with superimposed focusing gradient for high efficiency tapered X-ray FELs. North American Particle Acc. Conf. 509–511 (2019). https://doi.org/10.18429/JACoW-NAPAC2019-TUPLH10
24. M. Gehlot, G. Mishra, F. Trillaud et al., Magnetic design of a 14 mm period prototype superconducting undulator. Nucl. Instrum. Meth. A **846**, 13–17 (2017). https://doi.org/10.1016/j.nima.2016.11.070
25. J.H. Wei, Z.L. Chen, X.Z. Zhang et al., Numerical analysis of the end-field with correction coils for the superconducting undulator at IHEP. Nucl. Instrum. Meth. A **1026**, 166036 (2022). https://doi.org/10.1016/j.nima.2021.166036
26. Z.L. Chen, X.C. Yang, J.H. Wei et al., Vertical measurement and on-line correction of the magnetic field for a 1.5-m-long superconducting undulator. Nuclear Instrum. Meth. **1047**, 167826 (2023). https://doi.org/10.1016/j.nima.2022.167826
27. S. Casalbuoni, A. Bernhard, R. Frahm et al., One year operation of a superconductive undulator in the storage ring ANKA. AIP Conference Proceedings. 301–304. (2007). https://doi.org/10.1063/1.2436060

28. Z.L. Chen, X.Z. Zhang, X.C. Yang et al., Design and development of vacuum chamber for superconducting undulator at IHEP. Nucl. Instrum. Meth. A **1056**, 168713 (2023). https://doi.org/10.1016/j.nima.2023.168713
29. Y.Y. Liu, J. Wang, L. Wang et al., Design of cold mass supports for a superconducting undulator prototype at SINAP. IEEE T. Appl. Supercond. **25**, 4101004 (2015). https://doi.org/10.1109/TASC.2014.2386695
30. M.F. Xu, R. Ge, L. Bian et al., Design and research of cryostat for 3W1 superconducting wiggler magnet. IEEE T. Appl. Supercon. **28**, 4100906 (2018). https://doi.org/10.1109/TASC.2018.2790380
31. M.F. Xu, X.Z. Zhang, R. Ye et al., Design, assembly, and pre-commissioning of cryostat for 3W1 superconducting wiggler magnet. Nucl. Sci. Tech. **31**, 113 (2020). https://doi.org/10.1007/s41365-020-00816-4
32. J.H. Wei, Y.H. Li, X.C. Yang et al., Development and magnetic field measurement of a 0.5-m-long superconducting undulator at IHEP. J. Synch. Radiat. **29**, 997–1003 (2022). https://doi.org/10.1107/S1600577522006166
33. E.A. Anliker, Q.B. Hasse, Y. Ivanyushenkov et al., The design and manufacturing of superconducting undulator magnets for the advanced photon source upgrade. Proceedings of the 11th International conference on mechanical engineering design of synchrotron radiation equipment and instrumentation. 41–43 (2021). https://doi.org/10.18429/JACoW-MEDSI2020-MOPB09
34. J.H. Wei, X.C. Yang, X.Z. Zhang et al., Development and cryogenic test of superconducting undulator mock-up coils at IHEP. Nucl. Instrum. Meth. A **1034**, 166822 (2018). https://doi.org/10.1016/j.nima.2022.166822
35. E. Trakhtenberg, Y. Ivanyushenkov, M. Kasa, Evolution of the design of the magnet structure for the APS planar superconducting undulators. Proceedings of the North American Particle Accelerator Conference. (2016). https://doi.org/10.18429/JACoW-NAPAC2016-THPOA69
36. X.C. Yang, F.S. Chen, X.J. Sun et al., Study on the technology of 3W1 superconducting magnet. Radiat. Detect. Technol. Methods. **6**, 97–101 (2022). https://doi.org/10.1007/s41605-021-00302-4
37. X.J. Sun, F.S. Chen, X.C. Yang et al., Superconducting multipole wiggler with large magnetic gap for HEPS-TF. Nucl. Sci. Tech. **33**, 16 (2022). https://doi.org/10.1007/s41365-022-01001-5
38. N.N. Hu, K. Wang, H.M. Ma et al., R &D on glass fiber reinforced epoxy resin composites for superconducting Tokamak. Springerplus **5**, 1564 (2016). https://doi.org/10.1186/s40064-016-2995-6
39. X.Z. Zhang, M.F. Xu, X.C. Yang et al., Development of liquid helium-free cryostat for a superconducting undulator. Nucl. Instrum. Methods **1049**, 168037 (2023). https://doi.org/10.1016/j.nima.2023.168037
40. A. Grau, S. Casalbuoni, N. Glamann et al., Full-scale conduction-cooled superconducting undulator coils-Training, stability, and thermal Behavior. IEEE T. Appl. Supercon. **28**, 4100604 (2018). https://doi.org/10.1109/TASC.2018.2791927
41. Z.L. Chen, P. He, Y.H. Li et al., Magnetic field measurement system in vertical status for superconducting undulator cooled in Dewar. J. Instrum. **17**, T09008 (2022). https://doi.org/10.1088/1748-0221/17/09/T09008
42. Y. Ivanyushenkov, M. Abliz, C.L. Doose et al., Development status of a magnetic measurement system for the APS superconducting undulator. Proceedings of 2011 Particle Accelerator Conference, New York, NY, USA (2011), pp. 1286–1288. https://accelconf.web.cern.ch/PAC2011/papers/tup243.pdf
43. V.M. Tsukanov, S.V. Khrushchev, A.A. Volkov et al., Hall probe magnetic measurements of a superconducting undulator. Bull. Russ. Acad. Sci. Phys. **87**, 585–589 (2023). https://doi.org/10.3103/S1062873822701854